Two-body weak currents in heavy nuclei

E. M. Ney [1,*] J. Engel [1,†] and N. Schunck [2,‡]

[1] *Department of Physics and Astronomy, CB 3255, University of North Carolina, Chapel Hill, North Carolina 27599-3255, USA*

[2] *Nuclear and Chemical Science Division, LLNL, Livermore, California 94551, USA*

(Received 29 December 2021; accepted 7 March 2022; published 31 March 2022)

In light and medium-mass nuclei, two-body weak currents from chiral effective field theory account for a significant portion of the phenomenological quenching of Gamow-Teller transition matrix elements. Here we examine the systematic effects of two-body axial currents on Gamow-Teller strength and β-decay rates in heavy nuclei within energy-density functional theory. Using a Skyrme functional and the charge-changing finite amplitude method, we add the contributions of two-body currents to the usual one-body linear response in the Gamow-Teller channel, both exactly and though a density-matrix expansion. The two-body currents, as expected, usually quench both summed Gamow-Teller strength and decay rates, but by an amount that decreases as the neutron excess grows. In addition, they can enhance individual low-lying transitions, leading to decay rates that are quite different from those that an energy-independent quenching would produce, particularly in neutron-rich nuclei. We show that both these unexpected effects are related to changes in the total nucleon density as the number of neutrons increases.

DOI: 10.1103/PhysRevC.105.034349

I. INTRODUCTION

β decay is a well-studied weak process. Dating back to 1933, Fermi's theory of β decay [1] paved the way for our later understanding of the electroweak force. Despite substantial progress, however, a peculiar feature of nuclear β decay has puzzled physicists for decades. Gamow-Teller transition rates, the primary contributions to decay in most nuclei, are systematically overpredicted by the nuclear shell model [2], and a phenomenological "quenching factor" has been required to bring theoretical predictions in line with experimental data [3–5]. The physical source of the quenching was unclear until fairly recently.

The literature contains several reviews of the so-called quenching problem; recent examples include Refs. [6,7]. The work of Refs. [8–10] provides compelling evidence that in all but the lightest nuclei, where quenching is small, nuclear correlations and two-body meson-exchange currents each produce significant quenching. Nucleons contribute coherently to the two-body currents, which should therefore be important in heavy nuclei. Although *ab initio* many-body methods, with interactions and currents from chiral effective field theory (χEFT), have proved useful for studying the quenching problem in lighter nuclei, they are computationally difficult to apply in most heavy nuclei. Several studies of double-β decay and dark-matter scattering in medium-mass and heavy nuclei treated two-body currents in a simple nuclear-matter approximation [11–14], but a more complete treatment in heavy systems is still missing. Here we fill the gap.

Our approach is to use the χEFT currents in conjunction with a Skyrme energy functional. The simultaneous use of two distinct schemes is inconsistent, of course, but will do for an initial investigation of the effects of the two-body currents. Ultimately, we want to treat the numerical coefficients of the chiral currents as parameters to be fit in conjunction with the energy-density functional. We defer that large task to a future paper.

This paper is structured as follows: In Sec. II we discuss the weak axial current, its implementation in nuclear energy-density-functional (EDF) calculations of linear response, and a density matrix expansion of the two-body current. In Sec. III, we outline our method for numerically incorporating the two-body current in an axially-deformed oscillator basis. We then present calculations in several nuclei and discuss the effects of the new current in Sec. IV. Finally, in Sec. V, we discuss the outlook and conclude.

II. THEORETICAL MODEL

A. Weak axial current

β decay is a semileptonic process. It is governed by a Hamiltonian density that for energies much less than the mass of the W boson can be written as

$$H_\beta = -\frac{G_\beta}{\sqrt{2}} \int d^4x \, J_\mu(x) L^\mu(x) + \text{H.c.}, \tag{1}$$

where $G_\beta/(\hbar c)^3 = 1.14959 \times 10^{-5}$ GeV^{-2} can be inferred from superallowed decays [15], $J_\mu(x)$ is the nuclear weak current, $L^\mu(x)$ is the leptonic weak current, $x \equiv (\boldsymbol{x}, t)$, and we use the Einstein sum convention. With Fermi's golden rule in first-order perturbation theory, one computes decay rates from a phase-space-weighted transition matrix element.

*evan.ney@unc.edu
†engelj@unc.edu
‡schunck1@llnl.gov

Equation (1) implies that the β-decay transition matrix element between the initial atomic state $|I\rangle$ and the final state $|F\rangle$ is [16]

$$\langle F|H_\beta|I\rangle = -\frac{G_\beta}{\sqrt{2}}\, l^\mu \int d^3x\, \langle f|e^{-i\boldsymbol{q}\cdot\boldsymbol{x}} J_\mu(\boldsymbol{x})|i\rangle. \tag{2}$$

In this expression $\boldsymbol{q}$ is the momentum transferred to leptons and l^μ is a leptonic matrix element that depends only on initial and final lepton wave functions. The remaining term, $\langle f|J_\mu(\boldsymbol{x})|i\rangle$, is the matrix element of the nuclear current operator between initial and final nuclear states $|i\rangle$ and $|f\rangle$. Because nuclear states are complicated, the nuclear matrix elements cannot be written in closed form. Most often, one invokes the impulse approximation, which takes the nucleus to be a collection of free nucleons, so that the current is represented by a one-nucleon operator.

In the standard model, the nuclear current is a sum of vector and axial-vector pieces, $J_\mu(\boldsymbol{x}) = J^V_\mu(\boldsymbol{x}) + J^A_\mu(\boldsymbol{x})$. Here, we consider only the axial current in the limit of zero momentum transfer. The resulting leading-order contributions come from the spatial piece of the four-current. In the nonrelativistic impulse approximation this piece is a one-body vector operator with the first-quantized form

$$\boldsymbol{J}^A_{1\mathrm{b}}(\boldsymbol{x}) = -g_A \sum_i \boldsymbol{\sigma}^{(i)} t^{(i)}_\pm \delta^3(\boldsymbol{x} - \boldsymbol{r}_i). \tag{3}$$

The sum is over nucleons in the nucleus, $g_A \approx 1.27$ [17] is the axial-vector coupling, $\boldsymbol{x}$ is the position (a c-number argument of the quantum field operator $\boldsymbol{J}^A_{1\mathrm{b}}$), and $\boldsymbol{r}_i$ is an operator describing the location of the ith nucleon relative to the nuclear center of mass. We use the notation $\boldsymbol{\sigma}^{(i)} \equiv (\sigma^{(i)}_x, \sigma^{(i)}_y, \sigma^{(i)}_z)$ and $\boldsymbol{\tau}^{(i)} \equiv (\tau^{(i)}_x, \tau^{(i)}_y, \tau^{(i)}_z)$ for the usual Pauli matrices acting on the two-component spin and isospin vectors of the ith nucleon. We use $\boldsymbol{t}$ to denote the isospin operators themselves: $\boldsymbol{t}^{(i)} = \frac{1}{2}\boldsymbol{\tau}^{(i)}$. The raising/lowering operators in Eq. (5) are then $t^{(i)}_\pm = t^{(i)}_x \pm i t^{(i)}_y$. With this notation, $t_-|n\rangle = |p\rangle$, $t_+|p\rangle = |n\rangle$, and $t_-|p\rangle = t_+|n\rangle = 0$.

To go beyond the impulse approximation, we need to specify degrees of freedom. We take them to be given by χEFT, which treats only nucleons and pions explicitly, including other effects in contact interactions among the constituents. We restrict ourselves to the leading-order two-body axial current derived in Eqs. (A5) and (A6) of Ref. [18] (see also Refs. [19,20]). From those expressions, we derive the first-quantized two-body current operator, which has the form

$$\boldsymbol{J}^A_{2\mathrm{b}}(\boldsymbol{x}) = \sum_{i<j} \big[\mathcal{O}^{(2\mathrm{b})}_{ij}(\boldsymbol{r}_i - \boldsymbol{r}_j, \boldsymbol{p}_i)\, \delta(\boldsymbol{x} - \boldsymbol{r}_i) + \mathcal{O}^{(2\mathrm{b})}_{ji}(\boldsymbol{r}_j - \boldsymbol{r}_i, -\boldsymbol{p}_j)\, \delta(\boldsymbol{x} - \boldsymbol{r}_j)\big]. \tag{4}$$

We leave the operators $\mathcal{O}^{(2\mathrm{b})}$ unspecified for now, using them here just to indicate the form of the current. They depend on the coordinates of two nucleons and the momentum $\boldsymbol{p}_k = -\frac{i}{2}(\overrightarrow{\boldsymbol{\nabla}}_k - \overleftarrow{\boldsymbol{\nabla}}_k)$, which acts on wave functions of the kth nucleon.

We use the axial current operators in conjunction with Eq. (2) to generate a set of $\boldsymbol{x}$-independent operators whose nuclear transition matrix elements determine the decay probability. We begin by substituting Eqs. (3) and (4) in Eq. (2), and then evaluate the integral over $\boldsymbol{x}$. Using the long-wavelength (or allowed) approximation, we assume that $|\boldsymbol{q}|R$, where R is the nuclear radius, is small enough to let us replace $e^{-i\boldsymbol{q}\cdot\boldsymbol{x}}$ by unity. For the one-body part of the current, the procedure generates the operator

$$\boldsymbol{A}_{1\mathrm{b}} = -g_A \sum_i \boldsymbol{\sigma}^{(i)} t^{(i)}_\pm. \tag{5}$$

The two-body current contains a short-range (contact) piece and a finite-range pion-exchange piece. For the short-range part, after inserting explicit expressions for the operators $\mathcal{O}^{(2\mathrm{b})}$ in Eq. (4), we obtain

$$\boldsymbol{A}_{2\mathrm{b},s} = -\frac{g_A}{4m_N f_\pi^2} \sum_{i<j} [2\bar{d}_1 (t^{(i)}_\pm \boldsymbol{\sigma}^{(i)} + t^{(j)}_\pm \boldsymbol{\sigma}^{(j)}) + 4\bar{d}_2\, t^{(i\times j)}_\pm \boldsymbol{\sigma}^{(i\times j)}] \delta^3(\boldsymbol{r}_i - \boldsymbol{r}_j), \tag{6}$$

where s stands for "short," $\boldsymbol{\sigma}^{(i\times j)} \equiv \boldsymbol{\sigma}^{(i)} \times \boldsymbol{\sigma}^{(j)}$, $t^{(i\times j)}_\pm \equiv (\boldsymbol{t}^{(i)} \times \boldsymbol{t}^{(j)})_x \pm i(\boldsymbol{t}^{(i)} \times \boldsymbol{t}^{(j)})_y$, and to arrive at this expression we have inserted a missing factor of $-\frac{1}{4}$ [9,20,21] in the short-range term from Eq. (A6) of Ref. [18]. The finite-range pion-exchange two-body operator is

$$\boldsymbol{A}_{2\mathrm{b},\pi} = -\frac{g_A}{2m_N f_\pi^2} \Bigg\{ 4\bar{c}_3 \sum_{i<j} [t^{(j)}_\pm (\boldsymbol{\sigma}^{(j)} \cdot \boldsymbol{\nabla})\boldsymbol{\nabla} + t^{(i)}_\pm (\boldsymbol{\sigma}^{(i)} \cdot \boldsymbol{\nabla})\boldsymbol{\nabla}] + 2t^{(i\times j)}_\pm [\boldsymbol{p}_i (\boldsymbol{\sigma}^{(j)} \cdot \boldsymbol{\nabla}) + \boldsymbol{p}_j (\boldsymbol{\sigma}^{(i)} \cdot \boldsymbol{\nabla})] + 4\left(\bar{c}_4 + \frac{1}{4}\right) t^{(i\times j)}_\pm [(\boldsymbol{\sigma}^{(i)} \times \boldsymbol{\nabla})(\boldsymbol{\sigma}^{(j)} \cdot \boldsymbol{\nabla}) - (\boldsymbol{\sigma}^{(j)} \times \boldsymbol{\nabla})(\boldsymbol{\sigma}^{(i)} \cdot \boldsymbol{\nabla})] \Bigg\} Y_0(|\boldsymbol{r}_i - \boldsymbol{r}_j|). \tag{7}$$

This expression is equivalent to those given in Refs. [18,21], but is written entirely in terms of derivatives acting on the Yukawa function, $Y_0(r) = e^{-m_\pi r}/(4\pi r)$. The dimensionless low energy constants (LECs) in Eqs. (6) and (7) are defined by [18]

$$\bar{c}_i = m_N c_i, \qquad \bar{d}_i = \frac{m_N f_\pi^2}{g_A} d_i. \tag{8}$$

B. Linear response in energy-density-functional theory

Nuclear EDF theory away from closed shells is implemented through the Hartree-Fock-Bogoliubov (HFB) generalized mean field. To the extent that static HFB calculations approximate the exact energy and one-body density, the time-dependent HFB equations provide an adiabatic approximation to the full time evolution of the nuclear density, and the HFB

linear response is an adiabatic approximation to the exact response. The time-dependent equations can be written as [22]

$$i\dot{R}(t) = [\mathcal{H} + \mathcal{F}(t), R(t)], \quad R = \begin{pmatrix} \rho & \kappa \\ -\kappa^* & 1-\rho* \end{pmatrix}, \tag{9}$$

with ρ the one-body density matrix and κ the pairing tensor. In these equations, the mean-field Hamiltonian $\mathcal{H}$ and external field $\mathcal{F}$ take the forms

$$\mathcal{H} = \begin{pmatrix} t+\Gamma & \Delta \\ -\Delta^* & -(t+\Gamma)^* \end{pmatrix}, \quad \mathcal{F} = \begin{pmatrix} f+\widetilde{\Gamma} & \widetilde{\Delta} \\ -\widetilde{\Delta}^* & -(f+\widetilde{\Gamma})^* \end{pmatrix}. \tag{10}$$

The matrices t and f are from the kinetic piece of the Hamiltonian and the one-body external field, respectively. The terms Γ and Δ represent the effects of correlations. If the functional is associated with a (typically density-dependent) potential $\hat{V}$, and if the external field is generated in part, as it will be here, by a two-body operator $\hat{F}(t)$, these terms come from contracting the two-body matrix elements of $\hat{V}$ and $\hat{F}(t)$ with one-body density matrices:

$$\Gamma_{ik} = \sum_{jl} \bar{v}_{ijkl}\rho_{lj}, \quad \Delta_{ij} = \frac{1}{2}\sum_{ij} \bar{v}_{ijkl}\kappa_{kl},$$
$$\widetilde{\Gamma}_{ik} = \sum_{jl} \bar{F}_{ijkl}\rho_{lj}, \quad \widetilde{\Delta}_{ij} = \frac{1}{2}\sum_{ij} \bar{F}_{ijkl}\kappa_{kl}, \tag{11}$$

where the $\bar{v}$'s are antisymmetric matrix elements of $\hat{V}$ and the $\bar{F}$'s are antisymmetric matrix elements of $\hat{F}(t)$.

The HFB linear response comes from treating the time-dependent HFB equations in first order in the external field $\mathcal{F}(t)$ to obtain small oscillations around the static mean field. The oscillations are the same as those imposed by the quasiparticle random phase approximation (QRPA). One can obtain the linear response efficiently with the finite amplitude method (FAM) [23,24], the charge-changing version of which is outlined in several places [25–27]. Our work here takes advantage of the similarity between Γ and $\tilde{\Gamma}$ in Eq. (11) to include the effects of the two-body nuclear current operator in Eqs. (6) and (7). We neglect the "pairing field" $\widetilde{\Delta}$ in this paper and compute only the "particle-hole mean field" $\widetilde{\Gamma}$, which should be more important.

Our computation involves external perturbations that change the projection along the symmetry axis of the angular momentum by an amount K. In deformed nuclei each component of the vector operators in Eqs. (5)–(7) can induce a different response, but in systems where time-reversal symmetry is conserved the response to operators that change angular momentum by $\pm K$ is the same. The laboratory-frame response is a linear combination of the intrinsic responses to the different components of the vector operators, where each intrinsic result is multiplied by the factor $\Theta_K = 1\delta_{K,0} + \sqrt{2}\delta_{K,K>0}$ [28]. Because we therefore must compute the response to each component of the current operators, we refer to the external field as a vector, $\boldsymbol{\mathcal{F}}$, comprising $\boldsymbol{f}$, $\widetilde{\boldsymbol{\Gamma}}$, and $\widetilde{\boldsymbol{\Delta}}$. Equations (9)–(11) should be understood to represent the response to a single component of these vectors that changes intrinsic angular momentum by $K = 0, \pm 1$.

III. COMPUTATIONAL METHOD

We use the Python program PYNFAM [27] to compute β-decay properties. This program wraps the ground-state HFB solver HFBTHO [29–31] and the charge-changing FAM solver PNFAM [25] for computing the linear response. In all our calculations we use the same SKO′ Skyrme functional used in the global β-decay calculations of Refs. [27,32]. In fitting this functional, the authors took an effective value for g_A of 1.0, and considered one-body Gamow-Teller strength only.

Because of the similarity of Eqs. (9) and (10) to static HFB equations, we can implement the full two-body current in the FAM in a way that is very similar to the implementation of the finite-range Gogny interaction in HFB calculations [31]. This approach entails computing two-body matrix elements of the finite-range operator and contracting them with the one-body density, as in Eq. (11). Unlike the Gogny interaction, however, the two-body axial current is a charge-changing spin-dependent vector operator with a finite-range part that involves a Yukawa function (rather than a Gaussian).

A. Contact term

The zero-range term of the two-body current can be treated just like a Skyrme interaction. We express the contraction of the antisymmetrized current operator with the density matrix as

$$\widetilde{\boldsymbol{\Gamma}}_{ij,s} = \sum_{kl} \langle ik|\bar{\boldsymbol{A}}_{2b,s}|jl\rangle \rho_{lk}, \tag{12}$$

where $\bar{\boldsymbol{A}}_{2b,s} = \boldsymbol{A}_{2b,s}(1 - P^r P^\sigma P^\tau)$ is the antisymmetrized version of Eq. (6) and the matrix elements are given by

$$\langle ik|\bar{\boldsymbol{A}}_{2b,s}|jl\rangle = \int d^3\boldsymbol{r} \sum_{\sigma_1\sigma_1'\tau_1\tau_1'} \sum_{\sigma_2\sigma_2'\tau_2\tau_2'} \times \langle \boldsymbol{r}\sigma_1\tau_1\boldsymbol{r}\sigma_2\tau_2|\bar{\boldsymbol{A}}_{2b,s}|\boldsymbol{r}\sigma_1'\tau_1'\boldsymbol{r}\sigma_2'\tau_2'\rangle. \tag{13}$$

We can rewrite Eq. (12) in terms of the nonlocal densities [33,34],

$$\rho_{00}(\boldsymbol{r},\boldsymbol{r}') = \sum_{ij}\rho_{ji}\sum_{\sigma\tau}\phi_i^*(\boldsymbol{r}'\sigma\tau)\phi_j(\boldsymbol{r}\sigma\tau),$$
$$\rho_{1k}(\boldsymbol{r},\boldsymbol{r}') = \sum_{ij}\rho_{ji}\sum_{\sigma\tau\tau'}\phi_i^*(\boldsymbol{r}'\sigma\tau')\phi_j(\boldsymbol{r}\sigma\tau)\langle\tau|\tau_k|\tau'\rangle,$$
$$\boldsymbol{s}_{00}(\boldsymbol{r},\boldsymbol{r}') = \sum_{ij}\rho_{ji}\sum_{\sigma\sigma'\tau}\phi_i^*(\boldsymbol{r}'\sigma'\tau)\phi_j(\boldsymbol{r}\sigma\tau)\langle\sigma|\boldsymbol{\sigma}|\sigma'\rangle,$$
$$\boldsymbol{s}_{1k}(\boldsymbol{r},\boldsymbol{r}') = \sum_{ij}\rho_{ji}\sum_{\sigma\sigma'\tau\tau'}\phi_i^*(\boldsymbol{r}'\sigma'\tau')\phi_j(\boldsymbol{r}\sigma\tau)\langle\sigma|\boldsymbol{\sigma}|\sigma'\rangle\langle\tau|\tau_k|\tau'\rangle, \tag{14}$$

which are, respectively, the scalar-isoscalar, scalar-isovector, vector-isoscalar, and vector-isovector components of the full one-body density matrix. Then, evaluating the matrix elements of $\boldsymbol{A}_{2b,s}$, we can extract the direct mean field current $\widetilde{\boldsymbol{\Gamma}}_s^{\text{dir.}}(\boldsymbol{r})$,

$$\widetilde{\boldsymbol{\Gamma}}_s^{\text{dir.}}(\boldsymbol{r}) = \frac{g_A}{2m_N f_\pi^2}\left\{-\bar{d}_1\left[\rho_{00}(\boldsymbol{r})\boldsymbol{\sigma}t_\pm \mp \frac{1}{\sqrt{2}}\boldsymbol{s}_{1\pm1}(\boldsymbol{r})\right] -2i\bar{d}_2\boldsymbol{\sigma}\times\left[\boldsymbol{s}_{10}(\boldsymbol{r})t_\pm \pm \frac{1}{\sqrt{2}}\boldsymbol{s}_{1\pm1}(\boldsymbol{r})t_z\right]\right\}, \tag{15}$$

where the densities with one coordinate $\boldsymbol{r}$ are the diagonal elements of those defined in Eq. (14), and we have left the spin and isospin components of the field in operator form. When we compute matrix elements, we get

$$\widetilde{\boldsymbol{\Gamma}}^{\text{dir.}}_{ij,s} = \langle i|\widetilde{\boldsymbol{\Gamma}}^{\text{dir.}}_{s}(\boldsymbol{r})|j\rangle = \int d^3\boldsymbol{r} \sum_{\sigma\tau,\sigma'\tau'} \phi^*_i(\boldsymbol{r}\sigma\tau)\widetilde{\boldsymbol{\Gamma}}^{\text{dir.}}_{s}(\boldsymbol{r})\phi_j(\boldsymbol{r}\sigma'\tau'). \tag{16}$$

To obtain the exchange part of the mean field, we evaluate the matrix elements of $-\boldsymbol{A}_{2b,s}P^rP^\sigma P^\tau$ and extract the field

$$\begin{aligned}\widetilde{\boldsymbol{\Gamma}}^{\text{exc.}}_{s}(\boldsymbol{r}) = \frac{g_A}{2m_N f_\pi^2}\Bigg\{&\frac{1}{2}(\bar{d}_1 - 2\bar{d}_2)\left[\rho_{00}(\boldsymbol{r})\boldsymbol{\sigma}t_\pm \mp \frac{1}{\sqrt{2}}\boldsymbol{s}_{1\pm1}(\boldsymbol{r})\right]\\ &+\frac{1}{2}(\bar{d}_1 + 2\bar{d}_2)\left[\mp\frac{1}{\sqrt{2}}\boldsymbol{\sigma}\rho_{1\pm1}(\boldsymbol{r}) + \boldsymbol{s}_{00}(\boldsymbol{r})t_\pm\right]\\ &-i\bar{d}_1\left(\boldsymbol{\sigma}\times\left[\boldsymbol{s}_{10}(\boldsymbol{r})t_\pm \pm \frac{1}{\sqrt{2}}\boldsymbol{s}_{1\pm1}(\boldsymbol{r})t_z\right]\right)\Bigg\}.\end{aligned} \tag{17}$$

Finally, our HFB ground state is symmetric under time-reversal and does not include proton-neutron mixing. The spin and charge-changing ground-state densities therefore vanish, leading to the result

$$\widetilde{\boldsymbol{\Gamma}}_s(\boldsymbol{r}) \equiv \widetilde{\boldsymbol{\Gamma}}^{\text{dir.}}_{s}(\boldsymbol{r}) + \widetilde{\boldsymbol{\Gamma}}^{\text{exc.}}_{s}(\boldsymbol{r}) = -\frac{g_A}{4m_N f_\pi^2}\bar{c}_D\,\rho_{00}(\boldsymbol{r})\,\boldsymbol{\sigma}t_\pm. \tag{18}$$

Equation (18) is just as easy to work with as the usual one-body Gamow-Teller operator and depends on a single combination $\bar{c}_D \equiv \bar{d}_1 + 2\bar{d}_2$ of the LECs.

B. Finite-range term

To obtain the finite-range contribution to the mean field we must contract the antisymmetrized finite-range part of the current with the density matrix according to Eq. (11). The two-body current contains Yukawa functions, which are not separable. Without separability, the time it would take to compute the mean field in a model space with N harmonic oscillator shells would scale like $\mathcal{O}(N^{12})$, making large model spaces impossible [35].

However, we can approximate the Yukawa function by a sum of Gaussians. The two functions do not have the same behavior at $r = 0$ but the integrands in their matrix elements, which contain a factor of r^2, do. We therefore use the fit [36],

$$\begin{aligned}r^2\left[\frac{e^{-r}}{r}\right] \approx r^2[&6.79e^{-34r^2} + 2.41e^{-6.6r^2} + 0.786e^{-1.44r^2}\\ &+ 0.241e^{-0.38r^2} - 0.062e^{-0.15r^2} + 0.078e^{-0.13r^2}],\end{aligned} \tag{19}$$

to approximate two-body Yukawa matrix elements. The separability of Gaussian interactions makes contraction with the density in configuration space tractable. Because we perform our calculations in a basis of axially-deformed harmonic oscillator states, in which the mean field contains a Cartesian (z) component, contributing a computation time of $\mathcal{O}(N^8)$, and a radial (r, ϕ) component, contributing a time of $\mathcal{O}(N^{10})$, the separability provides vastly better computational scaling. Thus, we work with the nonlocal mean field $\widetilde{\boldsymbol{\Gamma}}_\pi(\boldsymbol{r}\sigma\tau, \boldsymbol{r}'\sigma'\tau')$. Spin and isospin degrees of freedom, however, are implicit in HFBTHO and PNFAM. It is therefore necessary to sum over the corresponding quantum numbers analytically. The result is then contracted over spatial quantum numbers numerically.

We compute Gaussian matrix elements in our axially deformed oscillator basis in the way described in Refs. [31,37], obtaining them as analytic functions of the oscillator quantum numbers, and using the Cartesian expansion of the radial oscillator wave functions to express the full Gaussian matrix elements entirely in terms of one-dimensional Gaussian matrix elements (i.e., with one-dimensional wave functions). The decomposition makes it easy to compute the derivatives in the two-body current. The finite-range terms in the current appear not as the Yukawa function $Y_0(r)$, but in the forms $\partial_i\partial_j Y_0(r)$ and $(\overleftarrow{\boldsymbol{\nabla}} - \overrightarrow{\boldsymbol{\nabla}})\partial_j Y_0(r)$. The derivatives acting on $Y_0(r)$ can be integrated by parts so that they act on wave functions, allowing us to use relations that relate derivatives of one-dimensional oscillator wave functions to linear combinations of a few other such wave functions. Thus, all finite-range matrix elements in $\widetilde{\boldsymbol{\Gamma}}_\pi$ are expressed as linear combinations of one-dimensional Gaussian matrix elements.

From now on we neglect the terms proportional to $\boldsymbol{p}_i$ and $\boldsymbol{p}_j$ in Eq. (7). They are computationally expensive to evaluate and contribute very little. In the nuclear-matter approximation of Refs. [11,13], for example, these terms change matrix elements by only 1.5%–2.5% in the zero-momentum limit for typical values of $2\bar{c}_4 - \bar{c}_3$. In addition, time-reversal symmetry causes the contributions of direct terms proportional to $\bar{c}_4$ to vanish exactly.

C. Density matrix expansion

To validate our implementation of the linear response produced by the two-body current, and to find good approximations to it, we compare it to the response produced by an effective density-dependent one-body current, derived from a kind of density matrix expansion (DME). The DME is a method to construct a density-dependent, *local* operator $O(\boldsymbol{r})$ that approximates the nonlocal operator $O(\boldsymbol{r}, \boldsymbol{r}')$ of interest [38–42]. When applied to a local, two-body, finite-range potential of the type $V(\boldsymbol{r}_1, \boldsymbol{r}_2)$, the DME effectively maps it into a local one-body potential $V(\boldsymbol{R})$ with $\boldsymbol{R} = \frac{1}{2}(\boldsymbol{r}_1 + \boldsymbol{r}_2)$. The application to a charge-changing current operator rather than a charge-conserving Hamiltonian introduces some subtleties that we describe along with details of the expansion in Appendix A. The DME leads to a more sophisticated density dependence for the one-body current than that given in Refs. [11] and [12].

At leading order, the DME reproduces the contact term exactly [cf. Eq. (18)]. As for the finite-range piece, the expansion produces no direct term at all at leading order. There is a leading-order exchange term, however, given by

$$\begin{aligned}&\widetilde{\boldsymbol{\Gamma}}^{\text{exc.}}_{\text{DME}}(\boldsymbol{r})\\ &= \frac{g_A}{m_N f_\pi^2}\boldsymbol{\sigma}t_\pm\Bigg\{\bar{C}\left[1 - m_\pi^2 F[k_F(\boldsymbol{r})] - \frac{1}{10}m_\pi^2 G[k_F(\boldsymbol{r})]\right]\rho(\boldsymbol{r})\\ &\quad -\bar{D}\rho(\boldsymbol{r}) - \frac{1}{6}\frac{\bar{C}m_\pi^2}{k_F^2(\boldsymbol{r})}G[k_F(\boldsymbol{r})]\left[\frac{1}{4}\nabla^2\rho(\boldsymbol{r}) - \tau(\boldsymbol{r})\right]\Bigg\},\end{aligned} \tag{20}$$

with $\bar{C} = \frac{1}{3}(2\bar{c}_4 - \bar{c}_3 + \frac{1}{2})$ and $\bar{D} \equiv \bar{d}_1 - 2\bar{d}_2$. Here $\rho(\boldsymbol{r})$ is the scalar-isoscalar particle density, $\rho(\boldsymbol{r}) \equiv \rho_{00}(\boldsymbol{r})$, and $\tau(\boldsymbol{r})$ is the (isoscalar) kinetic density, $\tau(\boldsymbol{r}) \equiv \boldsymbol{\nabla} \cdot \boldsymbol{\nabla}' \rho_{00}(\boldsymbol{r}, \boldsymbol{r}')|_{\boldsymbol{r}=\boldsymbol{r}'}$. The functions F and G are given by

$$F[k] = \frac{3}{2k^2}\left[1 - \frac{m_\pi}{k}\tan^{-1}\left(\frac{2k}{m_\pi}\right) + \frac{m_\pi^2}{4k^2}\ln\left(1+4\frac{k^2}{m_\pi^2}\right)\right],$$
$$G[k] = \frac{3}{2k^2}\left[1+8\frac{k^2}{4k^2+m_\pi^2} - \frac{m_\pi^2}{k^2}\ln\left(1+4\frac{k^2}{m_\pi^2}\right)\right], \quad (21)$$

and $k_F(\boldsymbol{r}) \equiv [3\pi^2\rho(\boldsymbol{r})/2]^{1/3}$ is the local Fermi momentum.

Although nonzero direct terms arise at higher orders (N^2LO, N^4LO, and beyond), the expansion of the direct term does not converge for a realistic pion mass. The DME for the direct current is essentially an expansion of a finite-range two-body object in delta functions and their derivatives [43], and the range of the pion is too large to allow the expansion to converge quickly at nuclear density. We therefore truncate the DME at leading order, in which the finite-range $\bar{c}_3$ contribution to the direct term vanishes completely. As we will see, however, this approximation is not bad.

IV. RESULTS

A. Modification of Gamow-Teller strength

In this section we explore the effects of the two-body axial current on the β^- transition strength function, which reduces to the Gamow-Teller strength distribution in the absence of two-body currents. We define a "bare" Gamow-Teller operator from Eq. (5) as $O_{\rm GT} \equiv \boldsymbol{A}_{1b}/g_A$, and add the two-body current to define a modified Gamow-Teller operator $O'_{\rm GT} \equiv O_{\rm GT} + (1/g_A)(\boldsymbol{A}_{2b,\pi} + \boldsymbol{A}_{2b,s})$. The bare Gamow-Teller transition strength from parent state $|i\rangle$ to daughter state $|f\rangle$ is then $B_{fi} \equiv |\langle f|O_{\rm GT}|i\rangle|^2$, and the full strength is $B'_{fi} \equiv |\langle f|O'_{\rm GT}|i\rangle|^2$. The charge-changing FAM computes the linear response to an external field operator and constructs the function $S(\omega)$. This function contains poles at excitation energies of the system with residues equal to the transition strengths. We obtain the derivative of, e.g., the full transition strength from the full FAM linear response, $S'(\omega)$, via [25]

$$g_A^2 \frac{dB'}{d\omega} = -\frac{1}{\pi}\,\mathrm{Im}[S'(\omega)]. \quad (22)$$

From the transition strength function we quantify the net two-body effect by defining the "total quenching factor,"

$$q \equiv \sqrt{\frac{\int d\omega \frac{dB'}{d\omega}}{\int d\omega \frac{dB}{d\omega}}}. \quad (23)$$

As the definition shows, q is determined by the ratio of the summed strengths, and is independent of g_A. The total quenching factor allows one to define an effective value of the axial-vector coupling, $g_A^{\rm eff} = q\, g_A$, that could be used in a one-body calculation to account for two-body effects. In general, those effects will depend on the transition, causing q to depend on the energy range of the integrals in Eq. (23). We therefore consider QRPA energies up to 60 MeV, which is generally sufficient to exhaust the β^- contribution to the Ikeda sum rule in the nuclei we consider.

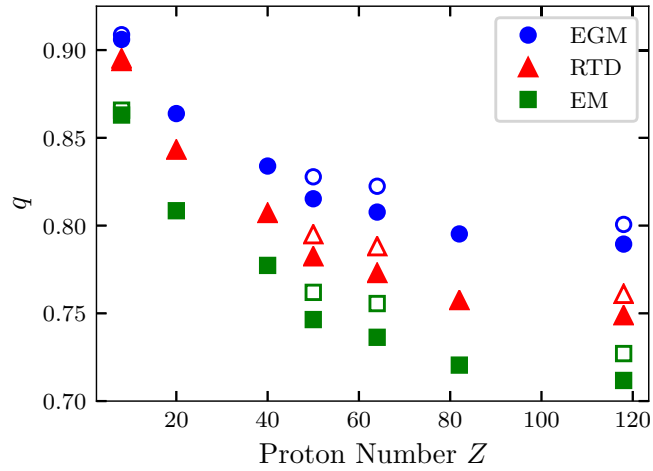

FIG. 1. Total quenching trends with proton number for the different sets of LECs in Table I, with $\bar{c}_D = 0$. The solid symbols correspond to the lightest isotope of a given element and the open symbols to the heaviest one, at the neutron drip line.

To begin our exploration of two-body currents in heavy nuclei we focus on a small set of nuclei, including the well-studied spherical isotopes ^{48}Ca, ^{90}Zr, and ^{208}Pb, plus, to examine the effects of neutron excess and deformation, the spherical isotopic chain ^{132}Sn – ^{174}Sn and the well-deformed isotopic chain ^{162}Gd – ^{220}Gd. We include only even-even isotopes and truncate the chains at the two-neutron drip line. Finally, to explore the effects of changes in the total mass, we include the light nuclei ^{20}O and ^{28}O, and the superheavy nuclei ^{294}Og and ^{388}Og. We find ^{28}O and ^{388}Og to be at the two-neutron drip line.

Figure 1 shows the value of q for all the nuclei in our data set except those in the middle of the isotopic chains. Because we use a density functional with no direct connection to the interactions and operators of χEFT, we consider three different sets of LECs for the long-range contribution to the current (see Table I) and at first ignore the contact coefficient $\bar{c}_D$. We find that the two-body current always has an overall quenching effect. For all LEC sets, the amount of quenching increases with proton number, leading to values of q between 0.86 and 0.91 in ^{20}O and between 0.73 and 0.80 in ^{388}Og. For elements at the boundaries of the isotopic chain, we also observe slightly less quenching in the heavier isotopes than the lighter ones. The differences in q between ^{20}O and ^{28}O are only 0.0014–0.0023, however, while the differences between the heaviest and lightest isotopes for Sn, Gd, and Og are all larger and similar, averaging 0.013–0.017.

TABLE I. A summary of the LECs used in this work. The entries all have units of GeV^{-1}.

Label	c_3	c_4
EGM [44]	−3.40	+3.40
RTD [45]	−4.78	+3.96
EM [46]	−3.20	+5.40

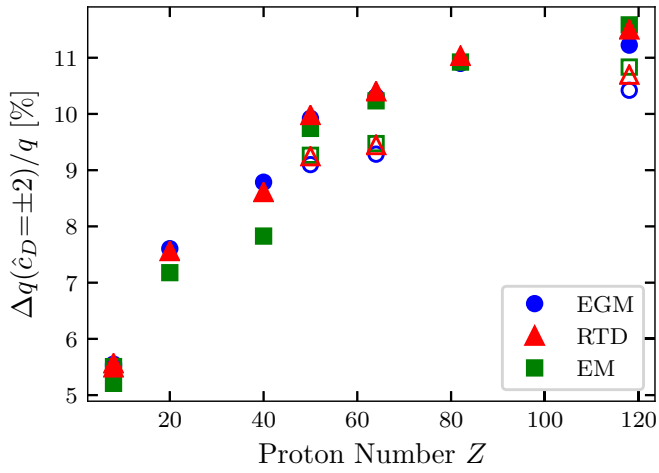

FIG. 2. Same as Fig. 1 but for the change in q with $\bar{c}_D = \pm 2$.

In Fig. 2 we examine the effect of the contact term. Equation (18) shows that adding a positive $\bar{c}_D$ reduces the quenching while adding a negative $\bar{c}_D$ increases it. The amount by which q is raised or lowered is almost symmetric about $\bar{c}_D = 0$, so the difference between the $\bar{c}_D = \pm 2$ values in Fig. 2 [denoted $\Delta q(\bar{c}_D = \pm 2)$] can be thought of as the size of error bars on the q values in Fig. 1 due to the variation of $\bar{c}_D$ in this range. The $\bar{c}_D$ contribution by itself is the same for all LEC sets; small differences in its effects reflect the interference of the contact with the finite-range term. The size of the variation due to $\bar{c}_D$ follows the same trends with N and Z as q itself, and ranges from 5% to 10% of q at $\bar{c}_D = 0$.

We compare calculations with the full current to those with the DME current in Fig. 3. The DME predictions—the circles in the figure—differ from those of the full current by roughly

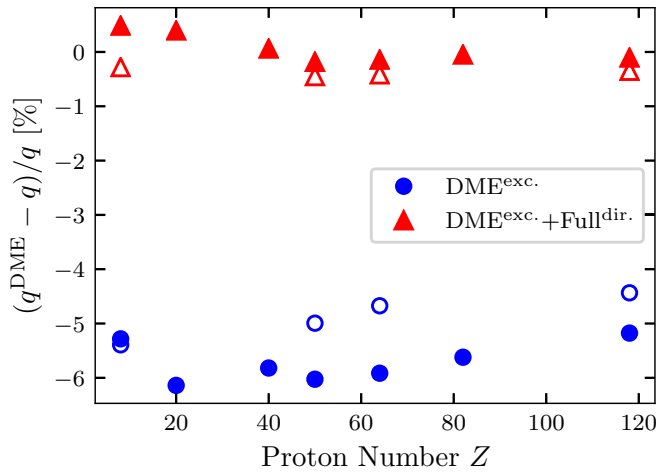

FIG. 3. The difference between the total quenching produced by the density-matrix expansion (DME) and by the full calculation, as a percentage of the full quenching with the RTD parameter set [45]. Blue circles correspond to predictions of the DME exchange current, not supplemented by anything else, while red triangles correspond to those of the DME exchange current together with the full direct current (see text).

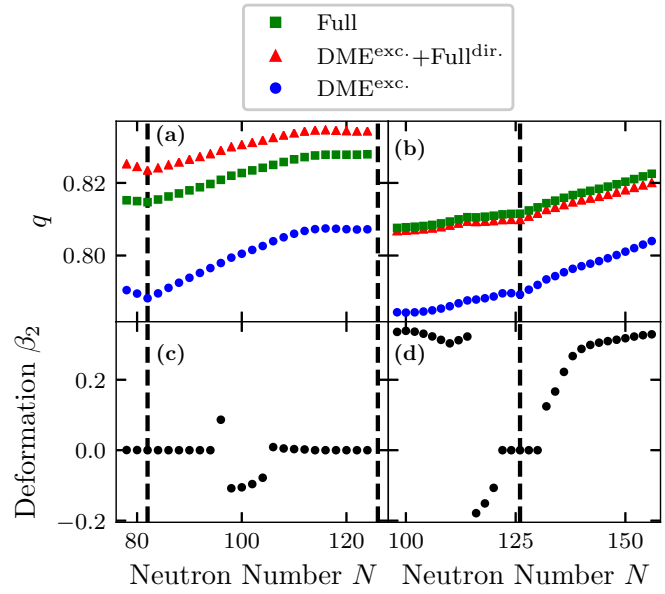

FIG. 4. Total quenching in the (a) Sn and (b) Gd isotopic chains with the EGM LEC set, and with the full current and the same versions of the DME shown in Fig. 3. Panels (c) and (d) show the respective deformations. Vertical lines indicate the magic numbers $N = 82$ and 126.

the same amount, ≈5%, for all nuclei. This indicates that the DME captures the same trends as in Fig. 1, but for all nuclei it overestimates the quenching slightly. The source of this discrepancy is the direct term, which is neglected in the DME. The triangles in the figure add the full current's direct term to the DME exchange term, producing a small correction that makes the agreement with the exact results almost perfect.

Next, we explore trends with deformation and neutron excess by computing the two-body contributions for all even-even isotopes of Sn and Gd from $N = 78$ to $N = 124$ (Sn) and $N = 98$ to $N = 122$ (Gd). We use the EGM LEC set with $\bar{c}_D = 0$, and again compare the full results with those of the DME. From Fig. 4(c) we see that the Sn nuclei are mostly spherical, though those in the middle of the shell are slightly deformed. On the other hand, Fig. 4(d) shows the Gd isotopes are very prolate, except right around the shell closure at $N = 126$. Although we see a small increase in quenching near the shell closures in both elements, there is no significant trend with deformation. There is, however, a small, continuous decrease in quenching with neutron excess that is also apparent in Fig. 1. The DME exchange term mirrors the full calculation, again slightly overestimating the quenching. We display its results because they are so much easier to compute than the full results. Like the nuclear-matter approximation of Refs. [11,13], the DME exchange expresses the two-body contribution as a density-dependent renormalization of the one-body Gamow-Teller operator. We thus expect the amount quenching to closely mirror the nuclear density.

B. Gamow-Teller rates

We turn now to β-decay rates. They have been measured in only a few of the nuclei in our set and, with the Skyrme

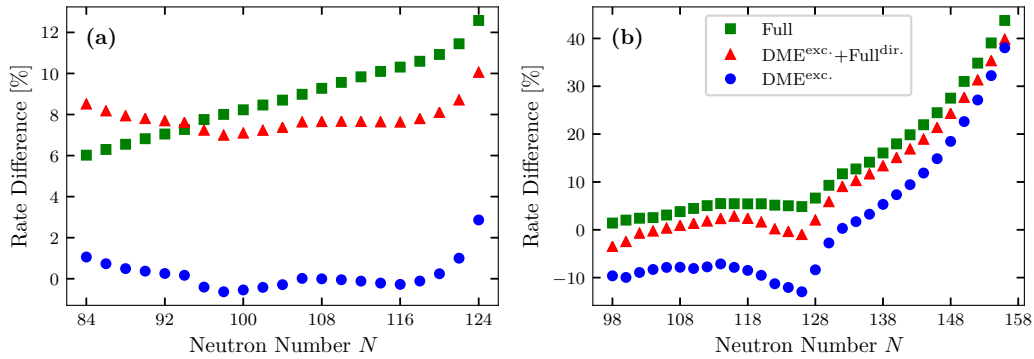

FIG. 5. Comparison of Gamow-Teller rates computed with the full one-plus-two-body current and $g_A = 1.27$ to those computed with the one-body current only and $g_A^{\text{eff}} = 1.0$, in (a) Sn and (b) Gd isotopes. The percent difference is $(\lambda^{\text{1b+2b}}_{g_A=1.27} - \lambda^{\text{1b}}_{g_A=1.0})/\lambda^{\text{1b}}_{g_A=1.0} \times 100\%$, with λ representing decay rates. The isotopes ^{128}Sn – ^{132}Sn are excluded because the Gamow-Teller strength below the β-decay threshold is negligible.

functional that we use, we under-predict those rates even without including a two-body current [27]. We are thus not able to see how much the two-body current will improve the description of rates without recalibrating the functional, perhaps even treating the LECs as free parameters, and examining more data. We leave that major task for a future publication. Here, however, we can still get an idea of what to expect by looking at the differences between rates computed with the one-body axial current and an effective axial-vector coupling $g_A^{\text{eff}} = 1.0$, employed in most EDF work so far (including Ref. [27]), and those computed with the one-plus-two-body axial current and the bare axial-vector coupling, $g_A = 1.27$. To what extent does a nucleus- and energy-independent effective g_A compensate for the omission of two-body currents?

We address the question in the Sn and Gd chains in Fig. 5, finding that in lighter isotopes the effective axial-vector coupling closely approximates the two-body current's effect on the rate. In very neutron-rich nuclei, however, we begin to see a more significant difference between the two approaches. The Sn isotopes show a steady increase in the difference with neutron number, with an uptick near the drip line to about 12%. In the lighter Gd isotopes, the difference is very small until the $N = 126$ shell closure, after which it increases markedly, to about 40% in ^{220}Gd. Although we do not plot the results, we have made the same rate comparison for the O and Og isotopes in our data set. In ^{20}O, the difference between the quenched one-body and unquenched one-plus-two-body rates is 32% and in ^{28}O it is 24%, a variation of only about 8%. But in ^{322}Og, the difference is 30% and in ^{388}Og it is 121%, a variation of over 90%. These findings suggest that a constant effective axial-vector coupling does not adequately account for the effects of two-body currents, particularly in very neutron-rich nuclei.

To understand the source of the discrepancy in neutron-rich isotopes, we examine the change in the low-lying one-body Gamow-Teller strength *distributions* (up to the β-decay threshold energy) caused by the two-body current for the lightest and heaviest Sn and Gd isotopes. This analysis is not so easy, unfortunately. The FAM requires that the strength distribution be computed with an artificial Lorentzian width applied to each transition, but the overlap of the Lorentzian tails from all transitions, in particular from the Gamow-Teller resonance, prevents us from using the strength for any one transition to compute the quenching factor for that transition. To get the best picture, we should use a very small artificial width to minimize the distortion. The FAM does not converge well if the width is too small, however, so we use a moderately small half-width of $\gamma = 0.1$ MeV to maintain sufficient numerical stability.

Figure 6 shows the resulting ratio of the one-plus-two-body strength to the one-body strength. The two-body current appears to affect all low-lying transitions in lighter isotopes in almost the same way, but in the heavier isotopes it appears to enhance some transitions. Such enhancement offsets the quenching of other transitions in the computation of q, explaining the significant underestimate made by the effective axial-vector coupling in these heavier nuclei.

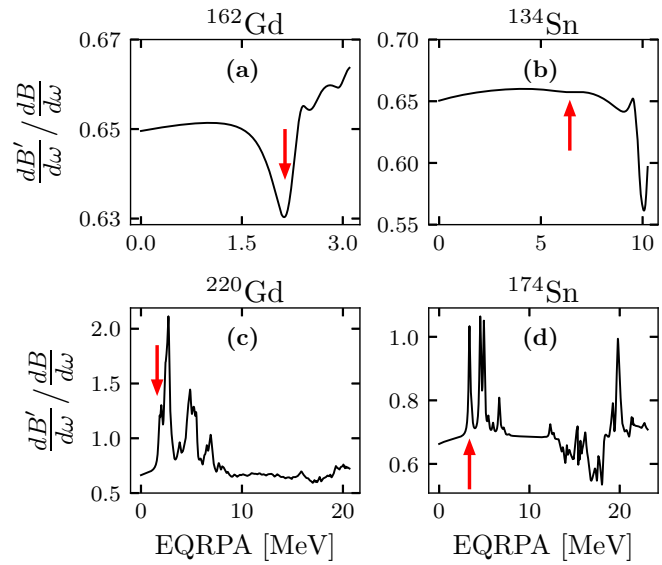

FIG. 6. Ratio of the one-plus-two-body FAM strength to the one-body strength for Gamow-Teller transitions below the β-decay threshold energy in the light isotopes (a) ^{162}Gd and (b) ^{134}Sn, as well as the heavy isotopes (c) ^{220}Gd and (d) ^{174}Sn. Arrows indicate the transitions examined in Figs. 7 and 8.

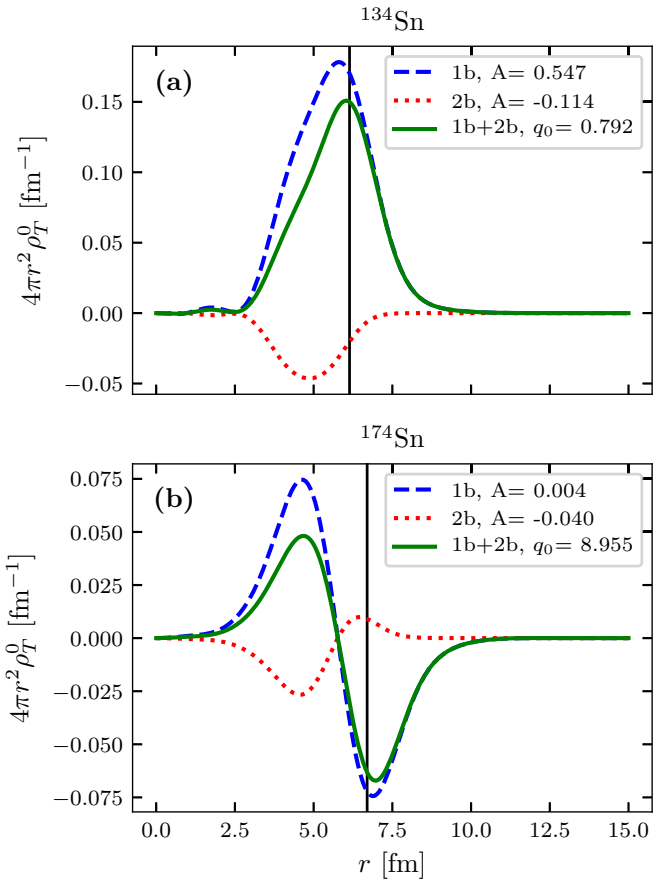

FIG. 7. Density of the lowest lying Gamow-Teller transition amplitude in (a) ^{134}Sn and (b) ^{174}Sn as a function of the radial coordinate r. The curves show densities for the one-body, two-body, and one-plus-two-body amplitudes. The factor of $4\pi r^2$ makes the integrated amplitudes equal to the areas under the curves. The vertical line is at the spherical radius $R_0 = 1.2A^{1/3}$, and the legends show the amplitudes A and quenching factors q_0 for the state in question. The overall signs of the amplitudes are arbitrary, but the relative signs between the one- and two-body terms are not. The quenching factor q_0 contains the square root of the squared amplitudes and is always positive.

What causes the enhancement of some low-lying transitions in neutron-rich isotopes? To answer, we compute the transition-amplitude density for the lowest lying states in the heaviest and lightest Sn isotopes with non-negligible rates. Although the quenching discrepancy in the Sn rates is not as large as in that in the Gd rates, the Sn isotopes are easier to understand because they are mostly spherical, allowing us to display the density as a function of a single variable. We use the DME to compute the densities because it provides a local one-body external field, while the field from the full current is nonlocal. (Details on the computation of transition densities in the FAM appear in Appendix B.) Figure 7 shows that the two-body current contributes very little at or beyond the nuclear surface. The reason is the nucleon-density dependence in Eq. (20) of the DME current field, which weakens quickly as the density falls. The falloff of the one-body curve is much slower. When the one-body contribution at the surface has the same sign as that in the interior, as in Fig. 7(a), this fact is not important and the two-body contribution quenches the transition amplitude. But when it has the opposite sign, leading to relatively small one-body transition strength, the difference between the quenching effect of the two-body current in the interior and its almost negligible effect at the surface causes the integrated matrix element to change sign and have a larger absolute value than without the two-body contribution, resulting in an enhanced strength.

As we already noted, enhancement is more common in neutron-rich nuclei than in those closer to stability. Although a careful and systematic analysis would be necessary to convincingly identify the physics responsible for the trend, the presence of a node in the transition-amplitude density associated with the space-independent operator $\boldsymbol{\sigma} t_-$—the condition that leads to enhancement by the two-body current—implies a mismatch between the shapes of neutron and proton single-particle wave functions with the same spatial quantum numbers. Such a mismatch is much more common in isotopes with a large neutron excess.

Most of the Gd isotopes are deformed, and an analysis of transition-amplitude densities is more complicated than in Sn because the density is not constant on spherical shells. Nevertheless, we can proceed. Figure 8 shows the density for a slice of the upper right quadrant of the nuclei, and we see that these deformed isotopes exhibit the same phenomena as the Sn isotopes: quenching when the one-body density has the same sign everywhere and enhancement when it changes sign, because of a smaller two-body contribution at the surface than in the interior. In the heavier isotope here, however, the surface contribution outweighs the interior contribution even at the one-body level. The concentration of the two-body contribution, with opposite sign, in the interior, makes the imbalance even larger and enhances the integrated transition strength.

Although in this exploratory paper we are not yet examining the consequences of the energy and isospin dependence of the quenching for total β-decay rates, our findings suggest that they will be significant.

V. CONCLUSIONS

We have developed a method to include the contributions of two-body charge-changing axial currents in the Skyrme-EDF linear-response, and applied the method to Gamow-Teller strength and β-decay rates. From the current, we construct mean-field-like external-field matrices that can easily be included in the linear response equations, e.g., through our charge-changing FAM. We have also developed a density matrix expansion for the two-body axial current. At leading order the expansion reproduces the contact current operator exactly and replaces the finite-range operator with a density-dependent one-body Gamow-Teller operator. This approximation reproduces the full linear response quite well for all the nuclei we studied, and provides a cheap way of including two-body contributions. If the direct term is computed exactly, an easier task in some codes than in our oscillator-based FAM, the expansion works almost perfectly.

To examine the effects on observables, we took the two-body current operators and the parameters that multiply them

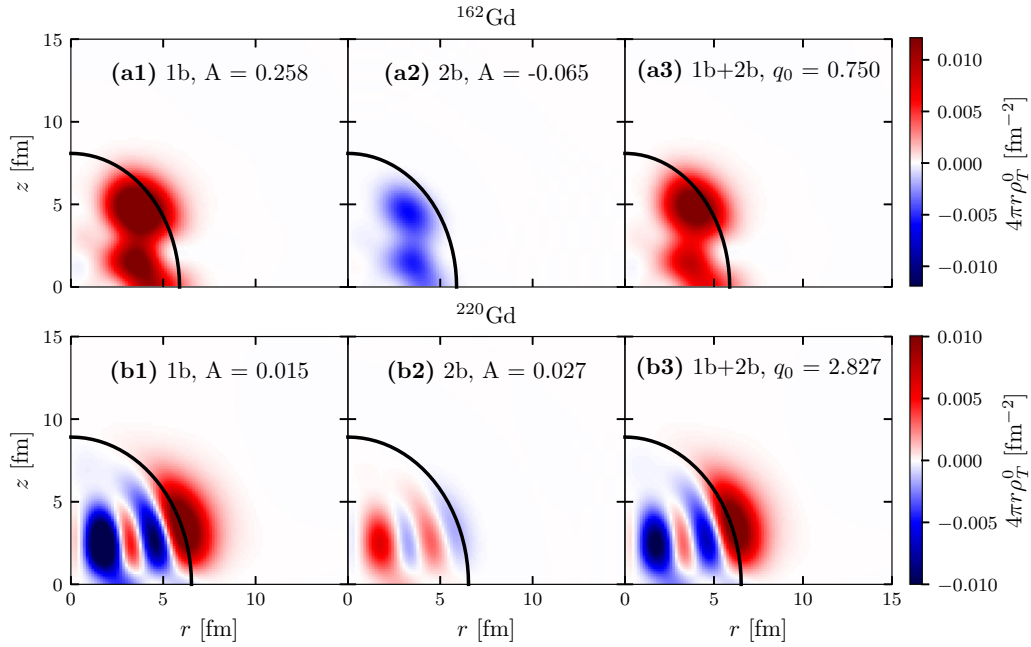

FIG. 8. Density of the lowest lying Gamow-Teller transition amplitude in (a) ^{162}Gd and (b) ^{220}Gd as a function of r and z. The figures show densities for the (a1,b1) one-body, (a2,b2) two-body, and (a3,b3) one-plus-two-body amplitudes. The volume element of $4\pi r$ is included (with an extra factor of 2 to account for the lower hemisphere). The curved lines indicate the nuclear surface determined from Eq. (B13), with $r = 1.2A^{1/3}$. The titles show the amplitudes A and quenching factors q_0 for the state.

from χEFT. We found, first, that in all the nuclei we studied the two-body current quenches the summed Gamow-Teller strength. The quenching increases significantly with Z and decreases with N. These trends can be understood by the density dependence of the effective one-body operator produced by the density-matrix expansion. We also looked at the energy dependence of the Gamow-Teller strength, finding that the two-body current causes a nearly constant quenching of decay to low-lying states near stability but a quenching with significant state dependence and in some cases even enhancement in very neutron-rich nuclei. Even though the amount of quenching of the summed strength changes just a little as N grows, the enhancement of low-lying strength can cause β-decay rates to differ significantly from what would be predicted by a single effective g_A. The energy dependence in neutron-rich nuclei, like the isospin dependence of the quenching of summed strength, is connected with nuclear density profiles and the occurrence of zeros in the spatial transition-amplitude distribution when the neutron excess is large.

Our results open up a number of interesting paths for future projects. Global calculations [27,32,47,48] indicate that first-forbidden β decay should be important in many nuclei, and our work should be extended to that channel and then applied to produce global calculations for r-process simulations. But most important is the marriage of χEFT with EDF theory. We have taken the first step here by including a chiral current together with a phenomenological density functional, in a way that is obviously not self consistent. It would make sense to refit not only the coupling constants of the functional but also the LECs in the currents. Once at least some of that is done, better systematic calculations of β-decay rates over the entire isotopic chart will become possible. Here the DME, which has already been applied to derive EDFs from chiral potentials [42,49] and has been used to obtain an analogous density-dependent current, will be especially useful. And with existing computational technology, one might be able work directly with two-and three-body chiral interactions and currents, without the DME. The combination of EDF phenomenology and methods with *ab initio* interactions and currents is promising and should be fully investigated.

ACKNOWLEDGMENTS

We thank L.J. Wang and R. Navarro-Perez for helpful correspondence regarding two-body currents and their numerical implementation. This work was supported in part by the Nuclear Computational Low Energy Initiative (NUCLEI) SciDAC-4 project under U.S. Department of Energy Grants No. DE-SC0018223 and No. DE-SC0018083, and by the Department of Energy under Grant No. DE-SC0013365 and the FIRE collaboration. Some of the work was performed under the auspices of the U.S. Department of Energy by Lawrence Livermore National Laboratory under Contract No. DE-AC52-07NA27344. Computing support came from the Lawrence Livermore National Laboratory (LLNL) Institutional Computing Grand Challenge program.

APPENDIX A: DENSITY MATRIX EXPANSION

Although one might start from a time-dependent energy-density functional that includes the effects of currents, the result of a DME will be the same as if we start with the "mean-field currents" $\widetilde{\mathbf{\Gamma}}_\pi$ and $\widetilde{\mathbf{\Gamma}}_s$. Instead of working with the

charge-changing density, as we would in an energy functional, we (equivalently) obtain the DME exchange functional by applying Eq. (24) from Ref. [39] directly to the products of single-particle wave functions [those corresponding to the single particle states i and j in, e.g., Eq. (12)] as well as to densities. Using the four-component spin-isospin vector $\Psi_i(\boldsymbol{r})$ in place of the individual components $\varphi_i(\boldsymbol{r},\sigma,\tau)$, we have

$$\begin{aligned}\Psi_i^\dagger(\boldsymbol{r}_1)\Psi_j(\boldsymbol{r}_2) &= e^{i\boldsymbol{r}\cdot\boldsymbol{k}}e^{\boldsymbol{r}\cdot\left[\frac{1}{2}(\nabla_1-\nabla_2)-i\boldsymbol{k}\right]}\Psi_i^\dagger(\boldsymbol{r}_1)\Psi_j(\boldsymbol{r}_2)|_{\boldsymbol{r}_1=\boldsymbol{r}_2=\boldsymbol{R}}\\ &\simeq e^{i\boldsymbol{r}\cdot\boldsymbol{k}}\left\{1+\boldsymbol{r}\cdot\left[\tfrac{1}{2}(\nabla_1-\nabla_2)-i\boldsymbol{k}\right]+\tfrac{1}{2}\left(\boldsymbol{r}\cdot\left[\tfrac{1}{2}(\nabla_1-\nabla_2)-i\boldsymbol{k}\right]\right)^2\right\}\Psi_i^\dagger(\boldsymbol{r}_1)\Psi_j(\boldsymbol{r}_2)|_{\boldsymbol{r}_1=\boldsymbol{r}_2=\boldsymbol{R}}. \end{aligned} \tag{A1}$$

Here $\boldsymbol{k}$ is a characteristic momentum, $\boldsymbol{r}\equiv\boldsymbol{r}_1-\boldsymbol{r}_2$, and $\boldsymbol{R}\equiv\frac{1}{2}(\boldsymbol{r}_1+\boldsymbol{r}_2)$.

For the decaying nucleon labeled by i and j, we take the characteristic momentum to have magnitude k_F. Assuming that the decaying nucleon is near the Fermi surface, working at the leading order in Eq. (A1) for the decaying-nucleon states $|i\rangle$ and $|j\rangle$—that is, neglecting all terms in the large braces except "1"—and averaging over angles for the momenta $\boldsymbol{k}$ (with the assumption that the system is spherically symmetric) gives

$$\Psi_i^\dagger(\boldsymbol{r}_1)\Psi_j(\boldsymbol{r}_2)\longrightarrow\Pi_1^s[k_F(\boldsymbol{R})r]\Psi_i^\dagger(\boldsymbol{R})\Psi_j(\boldsymbol{R}), \tag{A2}$$

with $\Pi_1^s[kr]\equiv j_0(kr)$ [39]. For the nucleon densities associated with φ_k and φ_l in Eq. (12), we use the expansion expressions from Ref. [39]. If, as for the full current, we neglect the terms in Eq. (7) that contain $\boldsymbol{p}_i$ and $\boldsymbol{p}_j$, the nonlocal spin density does not contribute and integrating the chiral current together with $\Pi_1^s[k_F(\boldsymbol{R})r]$ and the nucleon density from Eq. (26) of Ref. [39] over the relative coordinate $\boldsymbol{r}$ eliminates many of the other terms in Eq. (7). The integrals, together with the replacement of $\boldsymbol{R}$ by the one-body coordinate $\boldsymbol{r}$, result in Eq. (17). The expansion can be continued to higher order in both the wave functions of the decaying nucleon and the densities associated with the other nucleons, but we do not present the results of that analysis here.

The direct part of the current can also be expanded in the manner described in Ref. [43], where it was applied to the Gogny interaction. When used together with the chiral interaction, however, the expansion does not converge quickly, at least in our tests. We attribute the problems to the long range of pion exchange. In any event, in leading order the direct current does not contribute at all, so that the most of the effects of the two-body currents come from the exchange current.

APPENDIX B: TRANSITION DENSITIES

We wish to understand why the two-body current quenches some low-lying transitions and enhances others, particularly in neutron-rich nuclei. To do so, we compute the spatial density of the transition amplitude for particular transitions. A transition amplitude to a given state within the FAM depends on the corresponding QRPA eigenvector, which we must extract. Once we have it, we obtain the transition amplitude from

$$\langle m|F|0\rangle=\sum_{\mu<\nu}\left(X_{\mu\nu}^{m*}F_{\mu\nu}^{20}+Y_{\mu\nu}^{m*}F_{\mu\nu}^{02}\right), \tag{B1}$$

where the X's and Y's make up the QRPA eigenvector for state $|m\rangle$.

Reference [50] explains how the QRPA modes are related to the FAM response and shows that they can be determined up to an unknown phase, $e^{i\theta}=\langle m|\hat{F}|0\rangle/|\langle m|\hat{F}|0\rangle|$, from the expression

$$X_{\mu\nu}^m=e^{i\theta}\frac{\mathrm{Res}[X^{\mathrm{FAM}},\Omega_m]}{\sqrt{\mathrm{Res}[S,\Omega_m]}},\quad Y_{\mu\nu}^m=e^{i\theta}\frac{\mathrm{Res}[Y^{\mathrm{FAM}},\Omega_m]}{\sqrt{\mathrm{Res}[S,\Omega_m]}}, \tag{B2}$$

where Ω_m is the excitation energy of state $|m\rangle$, X^{FAM} and Y^{FAM} are the FAM amplitudes [24], S is the FAM response given, e.g., in Eq. (28) of Ref. [50], and $\mathrm{Res}[A,\Omega_m]$ is the residue of quantity A at frequency Ω_m. One can extract the residues of the FAM quantities from contour integrals, but it is difficult to choose a contour that contains only a single transition. A more efficient but more approximate method to extract the residues is to compute the FAM quantities a small distance γ above the real axis. The residue of S is then given by [51]

$$\mathrm{Res}[S,\Omega_m]\approx-\gamma\,\mathrm{Im}[S(\Omega_m+i\gamma)]. \tag{B3}$$

A similar relation holds for X^{FAM} and Y^{FAM} if we choose the undetermined phase such that the QRPA eigenvectors are real. To verify that the energy at which we are evaluating these functions is indeed a QRPA eigenvalue, and that the peak is well separated enough for the approximation in Eq. (B3) to hold, we compute the norm of the QRPA mode we extract:

$$N=\sum_{\mu<\nu}\left(X_{\mu\nu}^{m*}X_{\mu\nu}^m-Y_{\mu\nu}^{m*}Y_{\mu\nu}^m\right). \tag{B4}$$

If N is close to 1, we can be confident the results are close to the true QRPA values. The transitions highlighted in Fig. 6 all have values of $N>0.99$ for $\gamma=0.01$ MeV.

To obtain a spatial density for the transition amplitude we express Eq. (B1) in coordinate space. Because the mean fields for one-body and two-body currents are one-body operators, they have the simple form

$$\hat{F}=\sum_{ij}f_{ij}^{11}a_i^\dagger a_j, \tag{B5}$$

where $a_i^\dagger$ (a_i) creates (destroys) a particle in level i, and the (charge-changing) transition-amplitude density can be defined through the relation

$$\langle m|\hat{F}|0\rangle=\int d^3r\,\rho_T^m(\boldsymbol{r}), \tag{B6}$$

where, for β^- transitions,

$$\rho_T^m(r) = \sum_{\sigma,\sigma'} \int d^3r'\, \delta\rho^m(\boldsymbol{r}\sigma p, \boldsymbol{r}'\sigma' n) f^{11}(\boldsymbol{r}\sigma p, \boldsymbol{r}'\sigma' n). \quad \text{(B7)}$$

In Eq. (B7) the term $\delta\rho^m$ is the density perturbation for the mth QRPA mode in coordinate space, obtained through a change of basis,

$$\delta\rho^m(\boldsymbol{r}\sigma p, \boldsymbol{r}'\sigma' n) = \sum_{pn} \phi_p^*(\boldsymbol{r}'\sigma' p)\phi_n(\boldsymbol{r}\sigma n)\delta\rho_{pn}^m, \quad \text{(B8)}$$

where the $\phi_k(\boldsymbol{r}\sigma\tau) \equiv \psi_{n_r n_z}^{|\Lambda|}(r,z)\frac{e^{i\Lambda\phi}}{\sqrt{2\pi}}\chi_\Sigma(\sigma)\chi_q(\tau)$ are axially deformed oscillator basis states and the $\delta\rho_{pn}^m$ are given by the inverse Bogoliubov transformation,

$$\delta\rho_{pn}^m = U_{p\pi}X_{\pi\nu}^m V_{n\nu}^T - V_{p\pi}^* Y_{\pi\nu}^m U_{n\nu}^\dagger. \quad \text{(B9)}$$

Here $U_{p\pi}$ refers to the pth basis component of the πth proton quasiparticle state and $U_{n\nu}^\dagger$ refers to the nth basis component of the νth neutron quasiparticle state.

The full two-body current is nonlocal in position space, so we use the DME approximation to get a transition-amplitude density that depends on the local particle density. We then define a density-dependent function $g[\rho]$ such that the one-, two-, and one-plus-two-body current external fields can all be written in the form

$$f^{11}(\boldsymbol{r}\sigma\tau, \boldsymbol{r}'\sigma'\tau') = g[\rho(\boldsymbol{r})]\,\delta(\boldsymbol{r}-\boldsymbol{r}')\langle\sigma|\boldsymbol{\sigma}|\sigma'\rangle\langle\tau|t_-|\tau'\rangle \quad \text{(B10)}$$

with

$$g[\rho(\boldsymbol{r})] = \begin{cases} -1, & \text{one-body,} \\ f[\rho(\boldsymbol{r})], & \text{two-body,} \\ -1 + f[\rho(\boldsymbol{r})], & \text{one-plus-two-body,} \end{cases} \quad \text{(B11)}$$

and $f[\rho]$ the density-dependent function in Eq. (20).

Inserting Eqs. (B8) and (B10) into Eq. (B7) we obtain the transition-amplitude density in our axially deformed oscillator basis:

$$\rho_T^m(\boldsymbol{r}) = g[\rho(\boldsymbol{r})] \sum_{pn} \delta\rho_{pn}^m \psi_p(r,z)\psi_n(r,z)\langle\sigma_p|\boldsymbol{\sigma}|\sigma_n\rangle\delta_{\Lambda_p\Lambda_n}. \quad \text{(B12)}$$

The angular parts of the oscillator wave functions cause terms for which $\Lambda_p \neq \Lambda_n$ to vanish, so we have replaced them with a Kronecker delta to make the density real.

Finally, to construct radial plots for the two-dimensional axially symmetric density, we can average the density over shells defined by a spherical radius r and the deformation β_2,

$$S(r,\theta) = r\left[e^{-\frac{1}{2}\beta_2\sqrt{\frac{5}{4\pi}}}\cos(\theta) + e^{+\beta_2\sqrt{\frac{5}{4\pi}}}\sin(\theta)\right]. \quad \text{(B13)}$$

For spherical nuclei $\beta_2 = 0$, so the surfaces becomes spheres and the value of the density over the surfaces is constant.

[1] R. H. Stuewer, The seventh Solvay conference: Nuclear physics at the crossroads, in *No Truth Except in the Details: Essays in Honor of Martin J. Klein*, edited by A. J. Kox and D. M. Siegel (Springer, Dordrecht, 1995), pp. 333–362

[2] B. A. Brown and B. H. Wildenthal, Annu. Rev. Nucl. Part. Sci. **38**, 29 (1988).

[3] W.-T. Chou, E. K. Warburton, and B. A. Brown, Phys. Rev. C **47**, 163 (1993).

[4] G. Martínez-Pinedo, A. Poves, E. Caurier, and A. P. Zuker, Phys. Rev. C **53**, R2602 (1996).

[5] V. Kumar, P. C. Srivastava, and H. Li, J. Phys. G: Nucl. Part. Phys. **43**, 105104 (2016).

[6] J. T. Suhonen, Front. Phys. **5**, 55 (2017).

[7] J. Engel and J. Menéndez, Rep. Prog. Phys. **80**, 046301 (2017).

[8] S. Pastore, A. Baroni, J. Carlson, S. Gandolfi, S. C. Pieper, R. Schiavilla, and R. B. Wiringa, Phys. Rev. C **97**, 022501(R) (2018).

[9] P. Gysbers, G. Hagen, J. D. Holt, G. R. Jansen, T. D. Morris, P. Navrátil, T. Papenbrock, S. Quaglioni, A. Schwenk, S. R. Stroberg, and K. A. Wendt, Nat. Phys. **15**, 428 (2019).

[10] G. B. King, L. Andreoli, S. Pastore, M. Piarulli, R. Schiavilla, R. B. Wiringa, J. Carlson, and S. Gandolfi, Phys. Rev. C **102**, 025501 (2020).

[11] J. Menéndez, D. Gazit, and A. Schwenk, Phys. Rev. Lett. **107**, 062501 (2011).

[12] J. Menéndez, D. Gazit, and A. Schwenk, Phys. Rev. D **86**, 103511 (2012).

[13] P. Klos, J. Menéndez, D. Gazit, and A. Schwenk, Phys. Rev. D **88**, 083516 (2013).

[14] J. Engel, F. Šimkovic, and P. Vogel, Phys. Rev. C **89**, 064308 (2014).

[15] J. C. Hardy and I. S. Towner, Phys. Rev. C **102**, 045501 (2020).

[16] J. Walecka, in *Muon Physics* (Academic, New York, 1975), Chap. 5, pp. 113–218.

[17] P. Zyla *et al.* (Particle Data Group), Prog. Theor. Exp. Phys. **2020**, 083C01 (2020).

[18] T.-S. Park, L. E. Marcucci, R. Schiavilla, M. Viviani, A. Kievsky, S. Rosati, K. Kubodera, D.-P. Min, and M. Rho, Phys. Rev. C **67**, 055206 (2003).

[19] A. Baroni, L. Girlanda, S. Pastore, R. Schiavilla, and M. Viviani, Phys. Rev. C **93**, 015501 (2016).

[20] H. Krebs, E. Epelbaum, and U.-G. Meißner, Ann. Phys. (NY) **378**, 317 (2017).

[21] L.-J. Wang, J. Engel, and J. M. Yao, Phys. Rev. C **98**, 031301(R) (2018).

[22] P. Ring and P. Schuck, *The Nuclear Many-Body Problem* (Springer, 2004).

[23] T. Nakatsukasa, T. Inakura, and K. Yabana, Phys. Rev. C **76**, 024318 (2007).

[24] P. Avogadro and T. Nakatsukasa, Phys. Rev. C **84**, 014314 (2011).

[25] M. T. Mustonen, T. Shafer, Z. Zenginerler, and J. Engel, Phys. Rev. C **90**, 024308 (2014).

[26] T. Shafer, J. Engel, C. Frohlich, G. C. McLaughlin, M. Mumpower, and R. Surman, Phys. Rev. C **94**, 055802 (2016).

[27] E. M. Ney, J. Engel, T. Li, and N. Schunck, Phys. Rev. C **102**, 034326 (2020).

[28] A. Bohr and B. R. Mottelson, *Nuclear Structure: Nuclear Deformations* (World Scientific, Singapore, 1998), Volume II.
[29] M. V. Stoitsov, J. Dobaczewski, W. Nazarewicz, and P. Ring, Comput. Phys. Commun. **167**, 43 (2005).
[30] M. V. Stoitsov, N. Schunck, M. Kortelainen, N. Michel, H. Nam, E. Olsen, J. Sarich, and S. Wild, Comput. Phys. Commun. **184**, 1592 (2013).
[31] R. Navarro Pérez, N. Schunck, R. D. Lasseri, C. Zhang, and J. Sarich, Comput. Phys. Commun. **220**, 363 (2017).
[32] M. T. Mustonen and J. Engel, Phys. Rev. C **93**, 014304 (2016).
[33] N. Schunck, *Energy Density Functional Methods for Atomic Nuclei* (IOP, Bristol, 2019).
[34] E. Perlińska, S. G. Rohoziński, J. Dobaczewski, and W. Nazarewicz, Phys. Rev. C **69**, 014316 (2004).
[35] R. M. Parrish, E. G. Hohenstein, N. F. Schunck, C. D. Sherrill, and T. J. Martínez, Phys. Rev. Lett. **111**, 132505 (2013).
[36] J. Dobaczewski, W. Satuła, B. G. Carlsson, J. Engel, P. Olbratowski, P. Powałowski, M. Sadziak, J. Sarich, N. Schunck, A. Staszczak, M. Stoitsov, M. Zalewski, and H. Zdú Nczuk, Comput. Phys. Commun. **180**, 2361 (2009).
[37] W. Younes, Comput. Phys. Commun. **180**, 1013 (2009).
[38] J. W. Negele and D. Vautherin, Phys. Rev. C **5**, 1472 (1972).
[39] B. Gebremariam, T. Duguet, and S. K. Bogner, Phys. Rev. C **82**, 014305 (2010).
[40] S. K. Bogner, R. J. Furnstahl, H. Hergert, M. Kortelainen, P. Maris, M. Stoitsov, and J. P. Vary, Phys. Rev. C **84**, 044306 (2011).
[41] A. Dyhdalo, S. K. Bogner, and R. J. Furnstahl, Phys. Rev. C **95**, 054314 (2017).
[42] R. Navarro Pérez, N. Schunck, A. Dyhdalo, R. J. Furnstahl, and S. K. Bogner, Phys. Rev. C **97**, 054304 (2018).
[43] J. Dobaczewski, B. G. Carlsson, and M. Kortelainen, J. Phys. G: Nucl. Part. Phys. **37**, 075106 (2010).
[44] E. Epelbaum, W. Glöckle, and U.-G. Meißner, Nucl. Phys. A **747**, 362 (2005).
[45] M. C. M. Rentmeester, R. G. E. Timmermans, and J. J. de Swart, Phys. Rev. C **67**, 044001 (2003).
[46] D. R. Entem and R. Machleidt, Phys. Rev. C **68**, 041001(R) (2003).
[47] T. Marketin, L. Huther, and G. Martínez-Pinedo, Phys. Rev. C **93**, 025805 (2016).
[48] P. Möller, B. Pfeiffer, and K.-L. Kratz, Phys. Rev. C **67**, 055802 (2003).
[49] R. Navarro Pérez and N. Schunck, J. Phys.: Conf. Ser. **1308**, 012014 (2019).
[50] N. Hinohara, M. Kortelainen, and W. Nazarewicz, Phys. Rev. C **87**, 064309 (2013).
[51] E. Litvinova, P. Ring, and V. Tselyaev, Phys. Rev. C **75**, 064308 (2007).